Numerical Sensitivity Analysis of Divertor Heat Flux and Edge Temperature at DIII-D Under the Influence of Resonant Magnetic Perturbations

H. Frerichs[a*], O. Schmitz[a], D. Reiter[a], P. Cahyna[b], Y. Feng[c], T.E. Evans[d]

[a] *Institute of Energy and Climate Research (IEK-4), Forschungszentrum Jülich GmbH, Germany*

[b] *Institute of Plasma Physics AS CR, v.v.i., Association EURATOM/IPP.CR, Prague, Czech Republic*

[c] *Max-Planck-Institut für Plasmaphysik, Greifswald, Germany*

[d] *General Atomics, P.O. Box 85608, San Diego, California 92186-5608, USA*

Abstract

The impact of resonant magnetic perturbations on the edge plasma is investigated with the EMC3-EIRENE code. Earlier simulations have shown discrepancies to experimental observations regarding splitting of the divertor heat flux and reduction of the edge temperature. We demonstrate that the latter discrepancy is related to a possible overestimation of the classical parallel electron heat conductivity at low collisionalities. Furthermore, the heat flux splitting pattern can be modified through the application of an RMP screening model, while other model advancements - such as neutral gas pumping and re-fuelling, an 'ad hoc' flux limit or impurity radiation - seem to have no impact on the splitting pattern. A broadening and shape change of the toroidally averaged divertor heat flux is analyzed.

PACS: 52.25.Fi, 52.55.Rk, 52.65.-y, 52.65.Kj

keywords: DIII-D Divertor modelling, Edge modelling, Stochastic boundary

Corresponding author address: Wilhelm-Johnen-Str., 52425 Juelich, Germany

Corresponding author E-mail: h.frerichs@fz-juelich.de

Presenting author: Heinke Frerichs

Presenting author E-mail: h.frerichs@fz-juelich.de

1. Introduction

Resonant magnetic perturbations (RMPs) are a promising candidate for the control of edge localized modes (ELMs) in ITER according to successful demonstrations at present machines [1, 2, 3]. Already now, the study of ITER similar shape plasmas in the presence of RMPs is carried out at the DIII-D tokamak. Such scenarios are also investigated numerically with the EMC3-EIRENE code [4, 5], which is a 3D Monte Carlo transport code for the edge plasma (fluid transport model) in self-consistent interaction with neutral particles (kinetic transport model). The classical transport model by Braginskii [6] is applied for plasma transport along magnetic field lines, while anomalous cross-field transport is taken into account by a diffusion ansatz with free model parameters for the diffusion coefficients.

The 3D magnetic field structure, with or without RMP screening effects, is provided as input for the code: a field aligned grid is used for a fast reconstruction of magnetic field lines during transport simulations [7, 8]. Recent simulations for RMP H-mode plasmas at DIII-D have shown an explicit striation pattern in both particle and heat fluxes to the divertor target [9], but almost no heat flux striation is observed in the corresponding experiment [10]. Furthermore, a strong temperature reduction at the plasma edge by RMPs is found in simulations [11] (also with the E3D code [12]) but not in the experiment. These plasma discharges are characterized by a low divertor density and low collisionality, which suggests that kinetic corrections to the parallel electron heat conduction are probably necessary. In experiments with high collisionality, on the other hand, heat flux striation is indeed observed [13].

Possible reasons for these discrepancies are investigated: a more realistic treatment of neutral gas flow and recycling dynamics (2.A), the presence of impurity radiation (2.B), corrections to the classical parallel electron heat conductivity (2.C) and screening of RMPs by a plasma response (2.D). Then, in section 3, an analysis of the toroidally averaged target heat flux is given, which is of interest e.g. for fast rotating RMP fields.

2. Impact of model advancements on target heat flux and edge temperature

The following analysis is based on the ITER similar shape DIII-D discharge 132741 at $3760\,\mathrm{ms}$. This discharge is characterized by the following parameters:

toroidal magnetic field	$B_t = 1.8\,\mathrm{T}$
plasma current	$I_p = 1.5\,\mathrm{MA}$
edge input power	$P_{\mathrm{in}} = 6.3\,\mathrm{MW}$
elongation	$\kappa \approx 1.8$
average triangularity	$\delta \approx 0.5$
edge safety factor	$q_{95} = 3.52$
perturbation current	$I_c = 4\,\mathrm{kA}$

The perturbation field is provided by a set of six upper and lower rectangular coils located at the low field side of the machine. A configuration with even parity and toroidal mode number $n = 3$ is used. An overview of the magnetic configuration with vacuum RMP field is given in figure 1 (a) and (b).

Boundary conditions for the transport code are the edge input power P_{in} (i.e. total heating power minus core radiation, see table above) and the steady state pumping and re-fuelling rate $\Gamma_{\mathrm{in/out}} = 1.12 \times 10^{21}\,\mathrm{s}^{-1}$, both taken from experimental observations. Coefficients for anomalous particle, momentum and energy cross-field transport are set to $D_\perp = 0.2\,\mathrm{m}^2\,\mathrm{s}^{-1}$, $\eta_\perp = m_i\,n_i\,D_\perp$ and $\chi_{e\perp} = \chi_{i\perp} = 0.6\,\mathrm{m}^2\,\mathrm{s}^{-1}$, which is low enough to obtain a pronounced particle flux striation pattern [9].

A. Neutral gas pumping / re-fuelling

The neutral gas flow dynamics in the code has been improved towards a more realistic treatment, however, a new model parameter η_{pump} for the pumping quality had to be introduced [11] (i.e. the pump probability of particles crossing the *pump-surface*). Furthermore, the geometry of the pump duct/plenum is additional input. If the *pump surface* is defined at the entrance of the pump plenum (i.e. at the solid green line in figure 1 (a)), then a significant impact of η_{pump} on the divertor conditions is found (see solid boxes in figure 1 (c)). If, on the other hand, the pump plenum itself (or at least a large part of it as marked by the dashed lines in figure 1 (a)) is included in the simulations, then a much weaker impact of η_{pump} is found (see dashed boxes in figure 1 (c)). The "weak pumping"-solution is much closer to the "strong pumping"-solution in this case, and the latter is almost identical for the two *pump surface* configurations. Hence, the first (computationally much cheaper) pump configuration is consistent with rather strong pumping only.

In the following we use the first configuration and apply a moderately large value of $\eta_{\text{pump}} = 0.75$ (this is related to a pumping speed - i.e. the volume flow rate - of about $100\,\mathrm{m^3\,s^{-1}}$ for deuterium at a temperature of $300\,\mathrm{K}$). In any case, the impact of η_{pump} on the target heat flux (compare red and black dashed lines in figure 1 (e)) is negligible in this pump configuration. Note, however, that a separatrix temperature of $T_{e,\text{sepx}} \approx 180\,\mathrm{eV}$ is obtained in the "weak pumping" case which is much closer to the experimental observation than the value of $T_{e,\text{sepx}} \approx 600\,\mathrm{eV}$ of the "strong pumping" case. This is not necessarily an η_{pump} issue, but can e.g. be attributed to underestimated core radiation or additional edge power losses by impurities (see below).

B. Impurity radiation

We take into account local impurity radiation P_{imp} from sputtered carbon within a simple Corona model. Such a model has been introduced in [14] and is applied to assess the ITER

divertor performance under the influence of RMPs. The impurity density in this model is taken to be proportional to the main ion density, with a factor determined by a prescribed impurity radiation fraction f_{imp} so that:

$$\int dV \, P_{\text{imp}} \, = \, f_{\text{imp}} \, P_{\text{in}}. \tag{1}$$

The separatrix temperature drops from $T_{e,\text{sepx}}(f_{\text{imp}} = 0) \approx 600\,\text{eV}$ to $T_{e,\text{sepx}}(f_{\text{imp}} = 0.2) \approx 380\,\text{eV}$ and to $T_{e,\text{sepx}}(f_{\text{imp}} = 0.4) \approx 210\,\text{eV}$ (similar to the $\eta_{\text{pump}} = 0.1$ case from the previous paragraph), as can be seen in figure 1 (d). Divertor conditions change as well, i.e. there is a uniform reduction of the target heat flux, but there is no redistribution of heat flux from the outer to the inner peak (see figure 1 (e)). Further studies which include the production process and transport of impurities are required and ongoing. For the following paragraphs, however, we return to the configuration without impurities.

C. Limited parallel electron heat conduction

Another reason for the experimentally observed discrepancy between the particle and heat flux striation pattern might be related to the collisionality. E.g. the classical parallel electron heat conduction is overestimated at low collisionalities. A common way to account for this fact is the implementation of a limiting factor β in the effective heat conductivity $\kappa_{\parallel}^{e*} \, = \, \beta \cdot \kappa_{\parallel}^{e}$, which is obtained from a free streaming limit

$$\beta \, = \, \left(1 \, + \, \frac{\kappa_{\parallel}^{e} \, |\nabla_{\parallel} T_e|}{\alpha_e \, n_e \, v_{th} \, T_e} \right)^{-1}. \tag{2}$$

However, such an implementation requires the calculation of gradients of intrinsically (Monte Carlo) noisy data [15] - besides introducing a free model parameter α_e as well - and turned out to be unstable for this particular case. Therefore, we estimate the effect of a reduction of $\kappa_{\parallel}^{e}$ at low collisionalities by introducing an 'ad hoc' value for β. This factor can easily be introduced into a Monte Carlo scheme.

The impact of a constant reduction by 1, 2 and 4 orders of magnitude (although the latter is probably an unrealistically strong reduction) on the midplane profiles of electron temperature T_e and plasma density n is shown in figure 2 (a) and (b), respectively. It can be seen that it takes at least a reduction of 2 orders of magnitude to find a significant impact on T_e. If $\kappa_{\parallel}^{e}$ is reduced by 4 orders of magnitude, then the strong numerical 'energy pump-out' by the fast parallel transport is suppressed (which is consistent with experimental observations) and T_e is restored up to the axisymmetric level. As a consequence, the plasma pressure is increased which results in an increase of parallel particle transport (and consequently heat convection) and a weak reduction of plasma density. However, despite the strong impact on the electron temperature, there is no impact on the target heat flux q_t (see profiles in figure 2 (c) in comparison to the axisymmetric configuration). This demonstrates that there is a significant contribution from parallel heat convection at the target, otherwise a broadening of the footprint due to diffusion would be observed. Furthermore, there is no redistribution of heat flux between the outer and inner peaks, which is probably related to the oversimplified ansatz for β in this analysis.

D. Plasma response

An 'ad hoc' plasma response to an externally applied RMP field is taken into account by helical current sheets [16]. These current sheets are located at a selected set of magnetic flux surfaces and are tuned for maximal screening of the corresponding modes of the externally applied field on these surfaces (here: $m = 7 - 11$). We have previously demonstrated [17] that the size of the magnetic footprint diminishes with increasing screening and that this modification is reflected in the target fluxes. The secondary peaks shrink while the primary one increases towards the axisymmetric limit, as can be seen by the blue, dash-dotted line in figure 3 compared to the green, dashed line. This is a tendency towards experimental observations, however, the impact on the target particle flux is similar. Therefore we conclude that screening cannot be too

strong, because of clear experimental evidence regarding particle flux strike point splitting.

We now combine this screening case with the advancements of the last two paragraphs: either $40\,\%$ impurity radiation or a reduced el. heat conductivity is included. Similar to the results found above, there is no further redistribution of heat flux between the outer and inner peaks if either of these effects is included. Only a uniform reduction is found for the case with impurity radiation, while no particular change is found for the case with a reduction factor of 100 for the el. heat conductivity.

3. Averaged target heat flux profiles

An important issue of RMP application (e.g. as a prediction for smoothly rotating fields) is the modification of the toroidally averaged target heat flux

$$\overline{q}_t(L) \;=\; \frac{1}{2\,\pi}\,\int_0^{2\,\pi} d\varphi\, q_t(\varphi, L), \tag{3}$$

where L is the coordinate along the axisymmetric wall in the R-Z plane, starting from the unperturbed separatrix strike point. The target heat flux in the axisymmetric configuration is characterized by an exponential decay $\overline{q}_t \;=\; q_{t0}\,\exp\left(-L/\lambda\right)$. A fit to the simulation results allows to determine the e-folding length:

$$\lambda_{\text{axi}} \;=\; (2.03 \,\pm\, 0.02)\,\text{cm}. \tag{4}$$

The target heat flux in the (vacuum) RMP configuration, on the other hand, is characterized by a striation pattern which is guided by the perturbed separatrix with a maximal excursion of $L \,=\, 5.7\,\text{cm}$. Within this domain, the averaged heat flux is characterized by a linear decay $\overline{q}_t \;=\; q_{t0}\;(1 \,-\, L/\mathcal{L})$ with (see figure 4)

$$\mathcal{L}_{\text{RMP}} \;=\; (7.91 \,\pm\, 0.16)\,\text{cm}, \tag{5}$$

while an exponential decay with $\lambda_{\text{RMP}} = (2.25 \pm 0.05)\,\text{cm}$ is found only in the far SOL (i.e. beyond $L = 5.7\,\text{cm}$). A similar behavior is found for the plasma response case (with screening

on the $m = 7 - 11$ surfaces), although the main strike point region is smaller ($L \approx 2.5\,\mathrm{cm}$). This region is characterized by a linear decay with

$$\mathcal{L}_{\mathrm{m=7\text{-}11}} = (4.74 \pm 0.09)\,\mathrm{cm}. \tag{6}$$

An exponential decay is then again found in the far SOL with $\lambda_{m=7-11} = (2.10 \pm 0.04)\,\mathrm{cm}$. This broadening and weaker than exponential decay of the main strike point profile is consistent with other heat transport simulations for DIII-D [12].

4. Conclusions

We have investigated possible reasons for the discrepancies between experimental observations and simulation results regarding splitting of the divertor heat flux and reduction of the edge temperature at DIII-D. An overestimation of the classical parallel electron heat conductivity at low collisionalities has been investigated by means of an 'ad hoc' limit. The strong temperature drop found in the simulations in the presence of RMPs can be mitigated by such a limit, i.e. it demonstrates that the flat temperature profile in the absence of any flux limit is caused by fast parallel transport along open magnetic field lines. Furthermore, the heat flux splitting pattern can be modified through the application of an RMP screening model, while other model advancements - such as neutral gas pumping and re-fuelling, the above mentioned 'ad hoc' flux limit or impurity radiation - seem to have no impact on the splitting pattern. However, we conclude that screening cannot be too strong, because a similar redistribution of the particle flux is found as well and there is clear experimental evidence of particle flux strike point splitting. More realistic models of these effects are probably necessary to rule out their corresponding impact on the discrepancy with experimental observations. Finally, it has been shown that the toroidally averaged divertor heat flux is broadened by RMPs and that the exponential behavior is replaced by a linear decay in the region bounded by the separatrix.

Acknowledgments

This work was supported in part by the U.S. Department of Energy under DE-FC02-04ER54698 and the Grant Agency of the Czech Republic under Grant No. P205/11/2341.

References

[1] Evans T E, *et al.*, 2004 *Phys. Rev. Lett.* **92** 23 235003. doi: 10.1103/PhysRevLett.92.235003

[2] Liang Y, *et al.*, 2007 *Phys. Rev. Lett.* **98** 265004 1. doi:10.1103/PhysRevLett.98.265004

[3] Suttrop W, *et al.*, 2011 *Phys. Rev. Lett.* **106** 225004. doi:10.1103/PhysRevLett.106.225004

[4] Feng Y, *et al.*, 1997 *Journal of Nuclear Materials* **241-243** 930. doi:10.1016/S0022-3115(97)80168-7

[5] Feng Y, *et al.*, 2004 *Contrib. Plasma Phys.* **44** 1-3 57. doi:10.1002/ctpp.200410009

[6] Braginskii S, 1965 *Review of Plasma Physics* **1** 205

[7] Feng Y, *et al.*, 2006 *Nuclear Fusion* **46** 807. doi:10.1088/0029-5515/46/8/006

[8] Frerichs H, *et al.*, 2010 *Comp. Phys. Commun.* **181** 61. doi:10.1016/j.cpc.2009.08.016

[9] Frerichs H, *et al.*, 2010 *Nuclear Fusion* **50** 034004. doi:10.1088/0029-5515/50/3/034004

[10] Schmitz O, *et al.*, 2008 *Plasma Phys. Control. Fusion* **50** 124029. doi:10.1088/0741-3335/50/12/124029

[11] Frerichs H, *et al.*, 2012 *Nuclear Fusion* **52** 054008. doi:10.1088/0029-5515/52/5/054008

[12] Joseph I, *et al.*, 2008 *Nuclear Fusion* **48** 045009. doi:10.1088/0029-5515/48/4/045009

[13] Evans T E, *et al.*, 2007 *Journal of Nuclear Materials* **363-365** 570. doi: 10.1016/j.jnucmat.2006.12.064

[14] Feng Y, *et al.*, 2011 "EMC3-Eirene/SOLPS4.3 comparison for ITER" *Proc. 38th EPS Conf. on Plasma Physics (Strasbourg, France, 27 June - 01 July)* P-1.090

[15] Harting D, *et al.*, 2008 *Contrib. Plasma Phys.* **48**, No. 1-3, 99-105 doi: 10.1002/ctpp.200810017

[16] Cahyna P, *et al.*, 2011 *J. Nucl. Mater.* **415** S927. doi:10.1016/j.jnucmat.2011.01.117

[17] Frerichs H, *et al.*, 2012 *Phys. Plasmas* **19** 052507. doi:10.1063/1.4714616

Figure 1: (a) Poincaré plot of DIII-D discharge 132741. The wall-to-wall connection length L_c of magnetic field lines in the divertor region is color-coded. Pumping of neutral gas is taken into account by a pump surface (solid). An alternative implementation with an extended pump plenum is sketched by the dashed lines. (b) Magnetic footprint at the inner strike point (ISP). (c) Impact of the pumping quality η_{pump} on divertor conditions: strong pumping ($\eta_{\text{pump}} = 1.0$) vs. weak pumping ($\eta_{\text{pump}} = 0.1$). Solid boxes are obtained with a *pump surface* at the plenum entrance, while dashed boxes are obtained if the pump plenum is included in the simulations. (d), (e) Impact of impurity radiation ($0\,\%$, $20\,\%$ and $40\,\%$) on midplane temperature profiles and on the target heat flux at $\varphi = 0$ deg, respectively. Additional profiles for low pumping quality (using $f_{\text{imp}} = 0$) are shown as well.

Figure 2: Impact of a reduced el. heat conductivity on (a) midplane profiles of electron temperature, (b) plasma density and (c) on the target heat flux at the ISP at $\varphi = 0\,\text{deg}$. Axisymmetric profiles are shown for reference.

Figure 3: Target heat fluxes (at $\varphi = 0$ deg) for a case with RMP screening (blue) compared to the case without screening (green) and to the axisymmetric case (red). Furthermore, the same screening case with either $40\,\%$ impurity radiation (lightblue) or reduced el. heat conductivity (black) is shown.

Figure 4: Toroidally averaged target heat flux profiles for RMP configurations with and without screening compared to the axisymmetric configuration.

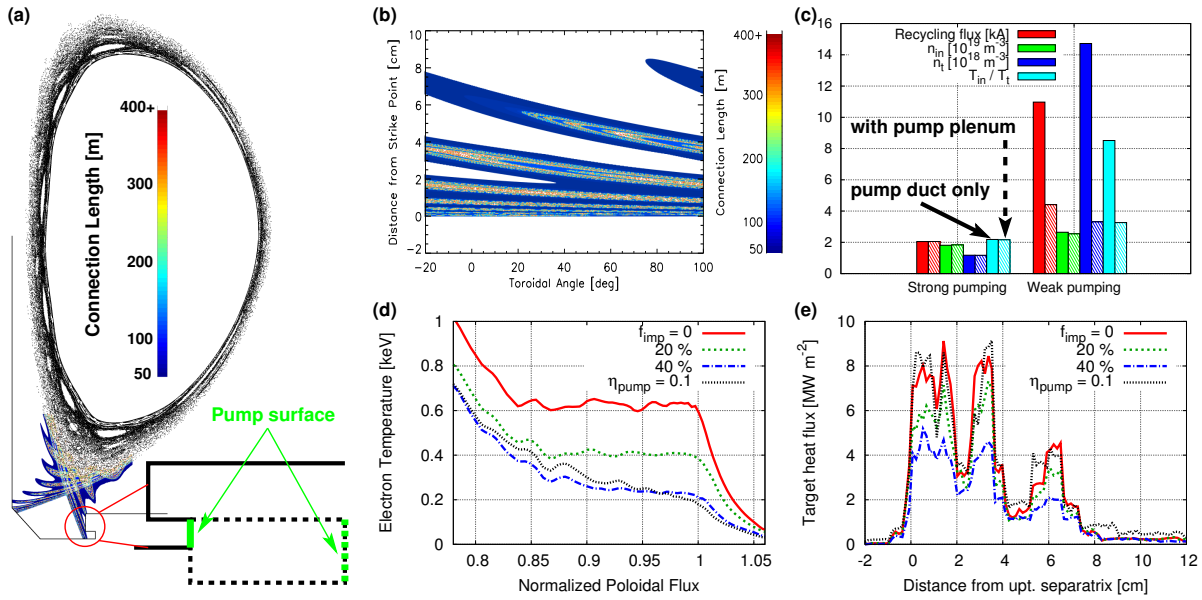
(a)
Connection Length [m]
400+
300
200
100
50
Pump surface
(b)
Distance from Strike Point [cm]
Toroidal Angle [deg]
Connection Length [m]
(c)
Recycling flux [kA]
n_{in} [10^{18} m^{-3}]
n_t [10^{18} m^{-3}]
T_{in} / T_t
with pump plenum
pump duct only
Strong pumping
Weak pumping
(d)
Electron Temperature [keV]
f_{imp} = 0
20 %
40 %
η_{pump} = 0.1
Normalized Poloidal Flux
(e)
Target heat flux [MW m^{-2}]
f_{imp} = 0
20 %
40 %
η_{pump} = 0.1
Distance from upt. separatrix [cm]

Figure 1

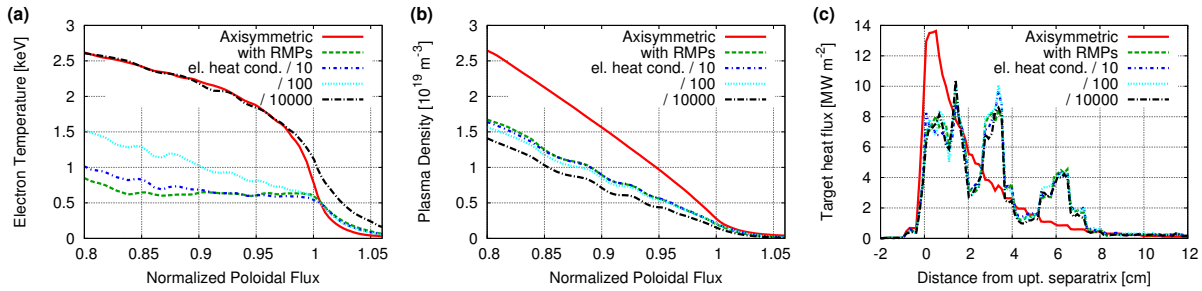
(a)
Electron Temperature [keV]
Normalized Poloidal Flux
Axisymmetric
with RMPs
el. heat cond. / 10
/ 100
/ 10000
(b)
Plasma Density [10^19 m^-3]
Normalized Poloidal Flux
Axisymmetric
with RMPs
el. heat cond. / 10
/ 100
/ 10000
(c)
Target heat flux [MW m^-2]
Distance from upt. separatrix [cm]
Axisymmetric
with RMPs
el. heat cond. / 10
/ 100
/ 10000

Figure 2

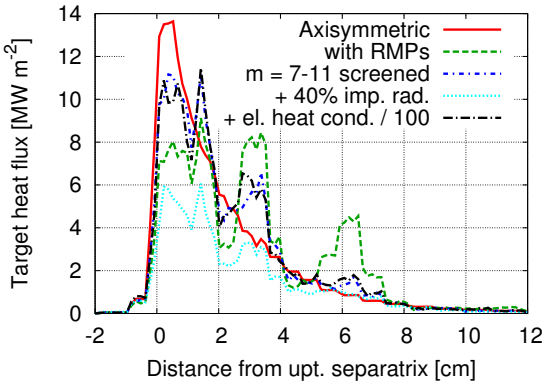
Target heat flux [MW m-2]
Distance from upt. separatrix [cm]
Axisymmetric
with RMPs
m = 7-11 screened
+ 40% imp. rad.
+ el. heat cond. / 100
14
12
10
8
6
4
2
0
-2
0
2
4
6
8
10
12

Figure 3

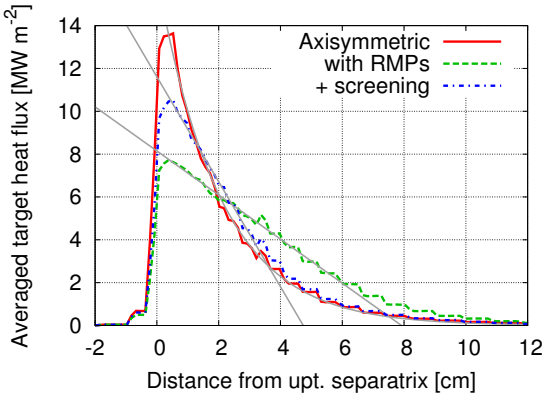
Averaged target heat flux [MW m-2]
Distance from upt. separatrix [cm]
Axisymmetric
with RMPs
+ screening
14
12
10
8
6
4
2
0
-2
0
2
4
6
8
10
12

Figure 4